

Enhanced photoluminescence of Tb^{3+} co-doped $La_2O_3:Bi^{3+}$ nanophosphors material using ethylene glycol route

PVSSSN Reddy, Ch.Satya Kamal, K.Sujatha, T.Samuel, M.Indiradevi¹,
Y.Rama Krishna² and K.Ramachandra Rao*

Crystal Growth and Nanoscience Research Centre,
Department of Physics, Government College (A), Rajahmundry-533105, A.P. India.

¹Department of Physics, Andhra University, Visakhapatnam-A.P, India

²Department of Engg.Physics, Andhra University, Visakhapatnam-A.P, India

Abstract: Mixed color photoluminescence (PL) was observed from Bi^{3+} and rare earth Tb^{3+} co-doped La_2O_3 ($La_2O_3:Bi^{3+}, Tb^{3+}$) prepared nanophosphor powder. The phosphor powders were prepared by polyol method using ethylene glycol as capping agent. The phase formation, functional groups identification of as prepared samples and morphological studies were confirmed by XRD, FTIR, scanning electron microscopy (SEM) and transmission electron microscopy (TEM). Colours of PL emissions widely changed from green-orange region to blue on heating $La_2O_3:Bi^{3+}, Tb^{3+}$ phosphor powders from 700 to 900 °C. The observed emission peaks in PL from phosphor powder materials were assigned to either the broad emission originating from the transition in Bi^{3+} or the visible emission peaks originating transition from the Tb^{3+} ions. All emission peaks of PL are plotted using CIE coordinates.

Keywords: Polyol method, Lanthanum oxide, Bismuth, Rare earth co-doping, Phosphorous, Photoluminescence.

1. Introduction

Research and development of nanoscale inorganic phosphors materials using binary oxides have attracted much attention in phosphors applications[1-5]. Among various materials, nanoscale phosphors doped with bismuth ions (Bi^{3+}) have extensively investigated because Bi^{3+} is to be good sensitizers of luminescence due to their band-like absorption character. In using rare-earth (RE) sesquioxides La_2O_3 , Y_2O_3 , Gd_2O_3 as host materials and doped with Bi^{3+} ions, it has been observed that blue-violet emissions originate from phosphors [6-8]. Lanthanum oxide (La_2O_3) is a semiconductor material [9] with the largest band gap among RE sesquioxides, with a value of 4.3 eV[10]. La_2O_3 crystallizes in the hexagonal system structure with space group $P\bar{3}m1$ [11]. Rare earth doped La_2O_3 phosphors have many potential applications in cathode ray tubes, field emission displays, plasma display panels, and vacuum fluorescent display devices [12]. Trivalent rare earth activated La_2O_3 phosphors have been extensively investigated due to their luminescent applications[13-16]. Photoluminescence (PL) and electroluminescence (EL) were observed from rare earth (RE^{3+}) co-doped $La_2O_3:Bi^{3+}$ ($La_2O_3:Bi^{3+}, RE^{3+}$) phosphor thin films[17]. Many synthesis techniques such as calcination methods [18], solutions combustion synthesis [19, 20, 21], conventional hydrothermal [22] and microwave hydrothermal methods [23] are used for preparation of La_2O_3 nanoparticles. Although terbium-doped La_2O_3 ($La_2O_3:Tb^{3+}$)

nanoparticles have been widely studied [24,25], to the best of authors knowledge La_2O_3 : Bi^{3+} , co-doped with Tb^{3+} ions nanoparticles synthesized by polyol route have not yet been investigated so far.

Polyol method can be used to prepare a variety of materials/compounds including metals, oxides, phosphates, sulphides, fluorides etc. having size in the range of few nanometres to micrometres. Essentially the preparation method involves the reaction of a polyol soluble salt of the metal ions and a precipitating agent. The method offers simple and economic method without using any hazardous or moisture sensitive reagents for preparing a variety of nanomaterials. In this paper, novel La_2O_3 : Bi^{3+} , Tb^{3+} nanoparticles were prepared successfully followed by annealing at 700 °C and 900 °C temperatures and their luminescent properties were discussed in detail.

2. Experimental details

2.1 Preparation of the nanoparticles

Starting materials, $\text{La}(\text{NO}_3)_3 \cdot 6\text{H}_2\text{O}$ [Merck, Germany], $\text{Bi}(\text{NO}_3)_3 \cdot 5\text{H}_2\text{O}$ [BDH Laboratory Chemicals Division, India], $\text{Tb}(\text{NO}_3)_3 \cdot 5\text{H}_2\text{O}$ [Sigma-Aldrich 99.99%] were used for the synthesis of nanoparticles. All the reagents were of AR and were used without further purification. Here, ethylene glycol is used as the capping agent and urea for hydrolysis. Initially La_2O_3 : Bi^{3+} (1at %) nanoparticles were prepared. Both $\text{La}(\text{NO}_3)_3 \cdot 6\text{H}_2\text{O}$ and $\text{Bi}(\text{NO}_3)_3 \cdot 5\text{H}_2\text{O}$ were dissolved in required amount of distilled water. To this solution, ethylene glycol (25 mL) was added and it was then transferred into a two-necked RB flask. The solution was slowly heated up to 100 °C followed by addition of 2 g of urea and the temperature was increased to 120 °C. At this temperature, the solution became turbid. The temperature was maintained at this value for 2 hours. The precipitate was collected after the reaction by centrifugation and then washed two times with acetone and three times with methanol followed by drying under ambient conditions. The samples prepared thus were finally heated to 700°C, 900°C in air at a heating rate of 10 °C per minute. The temperature was maintained at the respective values for duration of 5 hours. After that the furnace was switched off and the sample was subjected to natural cooling to room temperature. The same procedure was used for preparing the Tb^{3+} co-doped La_2O_3 : Bi^{3+} . Here in this paper the 1 at % bismuth content is kept constant and optimum 1 at% is reported for co-doping due to concentration quenching effect.

2.2 Characterization

X-ray diffraction (XRD) studies were carried out using a Philips powder X-ray diffractometer (model PW 1071) with Ni filtered $\text{Cu-K}\alpha$ radiation. The lattice parameters, unit cell volume were obtained from Rietveld refinement of the XRD patterns using POWDERX software. The average crystallite size was calculated from the diffraction line width based on Scherrer relation $D = 0.9\lambda/\beta\text{Cos}\theta$, where D is the average particles size, λ is the wavelength of X-rays and β is the corrected full width at half maximum (FWHM). All luminescence measurements were carried out at room temperature with a resolution of 5 nm, using Edinburgh Instruments FLSP 920 system attached with a 450 W Xe lamp as the excitation source. A micro second flash lamp was used for lifetime measurements. Morphological studies were carried out by Scanning Electron Microscopy (SEM) and Transmission Electron Microscopy (TEM) using a JEOL JEM 3000F TEM machine. IR patterns were recorded for a thin pellet of the La_2O_3 : Bi^{3+} , Tb^{3+} as prepared nanoparticles made with KBr using a Bomem MB102 machine.

3. Results and Discussions

3.1 XRD analysis

The phase of the as-prepared undoped $\text{La}(\text{OH})_3$ and doped samples was examined by XRD. Fig.1 (a) shows the XRD patterns of the pure $\text{La}(\text{OH})_3$ sample which all the diffraction peaks are attributed to the hexagonal crystal phase, which are in good agreement with the standard PCPDF card [13-0084] with the space group $\text{P6}_3/\text{m}$. Initially upon heating to 700 °C the XRD peaks became sharper because of an increase in crystallinity. With increasing temperature, it was deduced that $\text{La}(\text{OH})_3$ transforms to La_2O_3 . This XRD peaks shows the oxide nanoparticle phase which is in almost close agreement with hexagonal phase (PCPDF 83-1355) with the space group $\text{P}\bar{3}\text{m1}$ Fig.1 (b) [26].

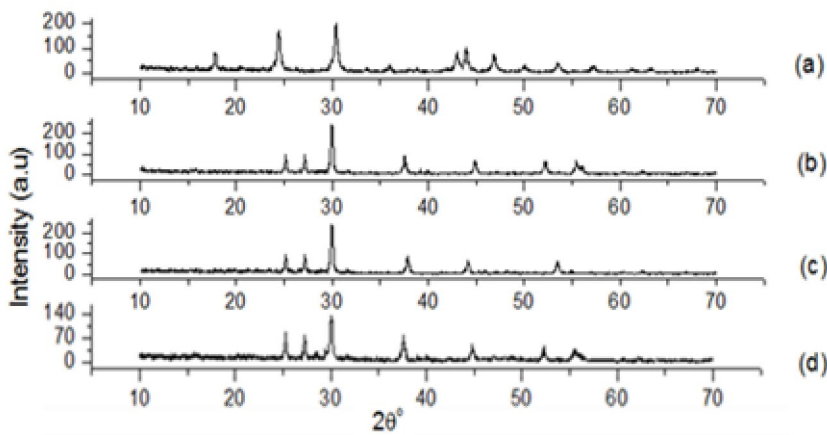


Fig.1 XRD Pattern for as prepared La_2O_3 (a) and 700 °C heated undoped La_2O_3 (b) $\text{La}_2\text{O}_3:\text{Bi}^{3+}$ (c) Co-doped with (d) Tb^{3+}

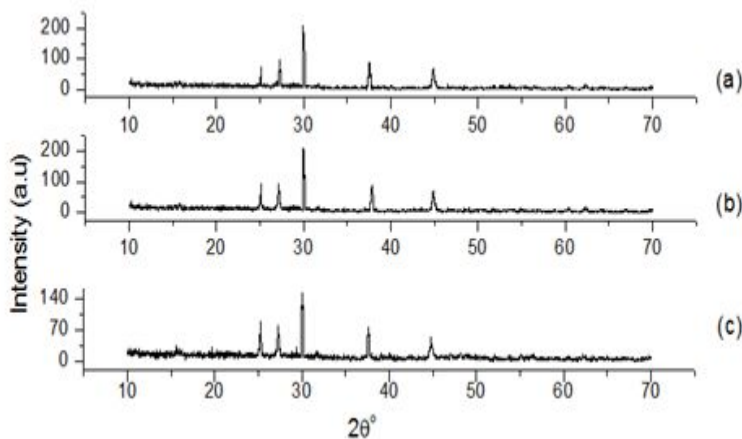


Fig.2 XRD Pattern for 900 °C heated undoped La_2O_3 (a) $\text{La}_2\text{O}_3:\text{Bi}^{3+}$ (b) Co-doped with (c) Tb^{3+}

All the remaining XRD patterns for $\text{La}_2\text{O}_3:\text{Bi}$ doped and rare earth co-doped samples Fig 1. (c and d) are indexed with the hexagonal form of La_2O_3 . For getting pure hexagonal crystal structure, high temperature heating is done at 900 °C. Hence pure hexagonal phase is attributed with better crystallinity Fig.2 (a-c). No diffraction peaks of other impurities were detected, even when co-doping is done to $\text{La}_2\text{O}_3:\text{Bi}^{3+}$. From Figs.1 and 2 a slight shift in peaks is observed due to co-doping. All of these results explain that the doped Tb^{3+} and Bi^{3+} ions completely enter into the matrix and occupy La^{3+} sites in these phosphors. According to the Scherrer's equation, the average crystallite size of heated samples is estimated to be 32- 41nm. The cell parameters of the heated samples at 700 °C and 900 °C have also been determined by X-ray diffraction and refined using the POWDERX software. The cell parameters calculated were listed in Table.1 minor changes are observed in lattice parameters on co-doping. Lattice parameters of La_2O_3 for reference are $a = 4.057 \text{ \AA} = b$ and $c = 6.430 \text{ \AA}$.

Table.1 Cell Parameters of heated samples.

Sample	700 °C Heated				900 °C Heated			
	a (Å)	b (Å)	c (Å)	V(cc)	a (Å)	b (Å)	c (Å)	V(cc)
Undoped La_2O_3	4.021(3)	4.021(3)	6.541(3)	91.63	4.023(3)	4.023(3)	6.552(3)	91.44
$\text{La}_2\text{O}_3:\text{Bi}^{3+}$	4.018(8)	4.018(8)	6.497(8)	90.54	4.026(2)	4.026(2)	6.517(3)	91.31
$\text{La}_2\text{O}_3:\text{Bi}^{3+},\text{Tb}^{3+}$	4.026(4)	4.026(4)	6.510(4)	91.46	4.022(4)	4.022(4)	6.505(4)	91.16

3.2 Structural and morphological studies

3.2.1 SEM images

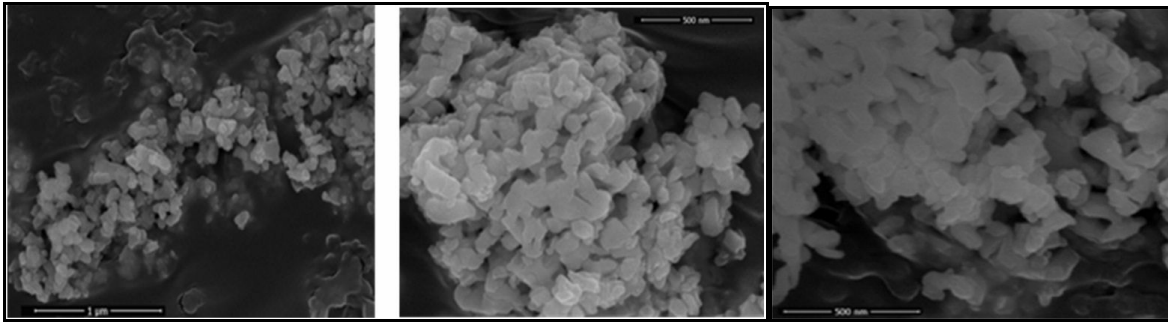
(a)Undoped La_2O_3 (b) $\text{La}_2\text{O}_3: \text{Bi}^{3+}$ (c) $\text{La}_2\text{O}_3: \text{Bi}^{3+}, \text{Tb}^{3+}$

Fig.3 SEM images of La_2O_3 700 °C heated Undoped and Doped Samples

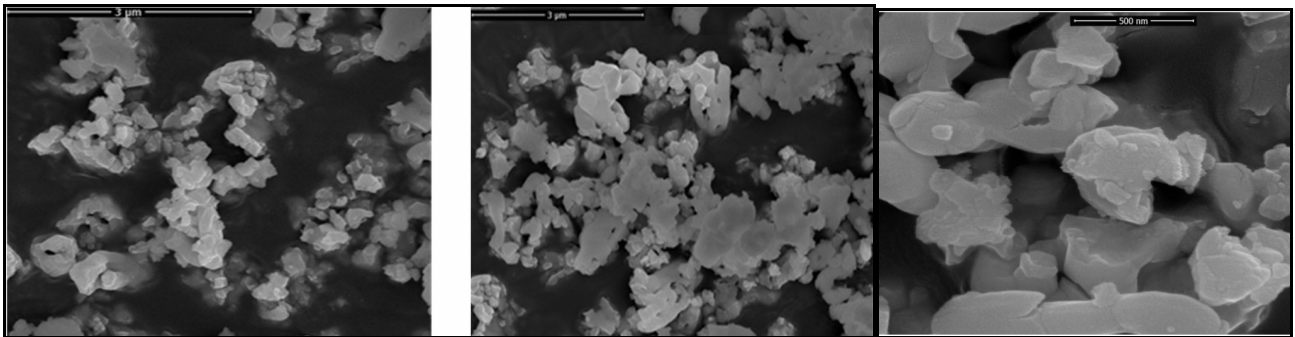
(a)Undoped La_2O_3 (b) $\text{La}_2\text{O}_3: \text{Bi}^{3+}$ (c) $\text{La}_2\text{O}_3: \text{Bi}^{3+}, \text{Tb}^{3+}$

Fig.4 SEM images of La_2O_3 900 °C heated Undoped and Doped Samples

The surface morphology and crystallinity of solid host materials are important parameters which determine the emission characteristics of phosphors. The morphological analysis of La_2O_3 , $\text{La}_2\text{O}_3:\text{Bi}^{3+}$ and Tb^{3+} co-doped heated at 700 and 900 °C samples was performed by SEM examination shown in Figs 3 and 4. It can be seen from images the samples are of sphere-like structure. From these images it is clear that the aggregation and particle sizes of the $\text{La}_2\text{O}_3: \text{Bi}^{3+}$ increases with rare earth co-doping. Also, it is clearly seen that the particles are in the agglomerated form with their size in the micrometer range.

3.2.2 TEM images

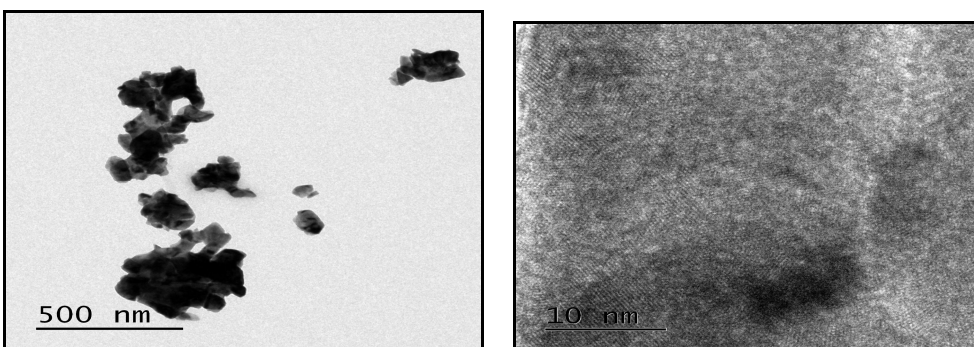


Fig. 5 (a)TEM image (b) HRTEM of 700 °C $\text{La}_2\text{O}_3: \text{Bi}^{3+}, \text{Tb}^{3+}$ phosphors material

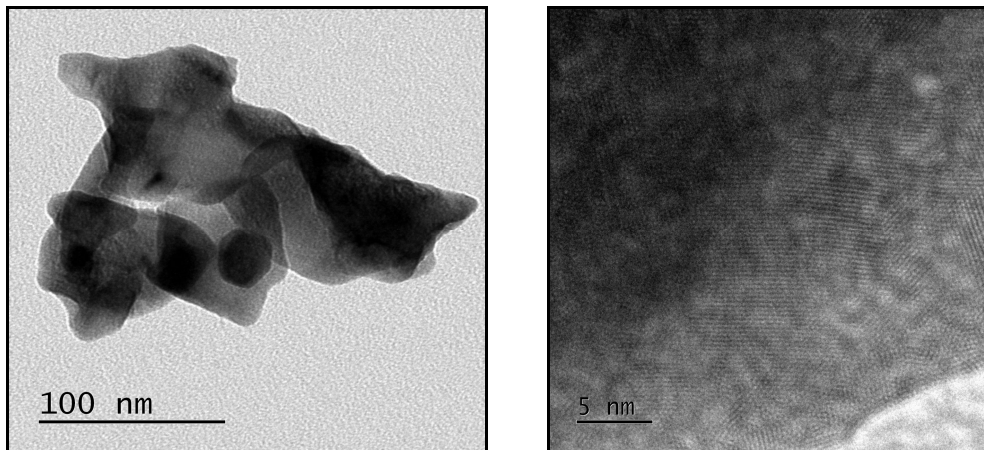
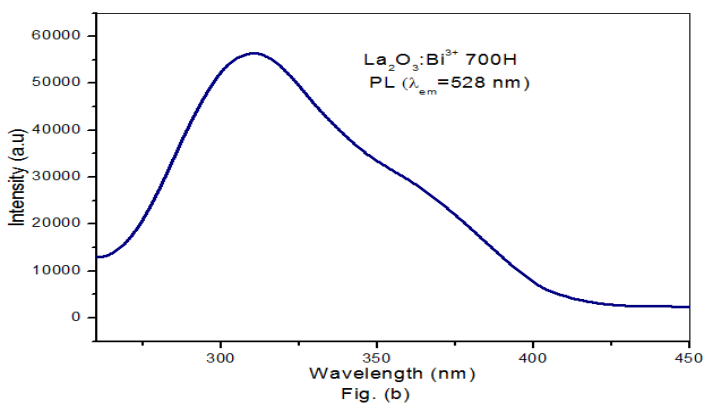
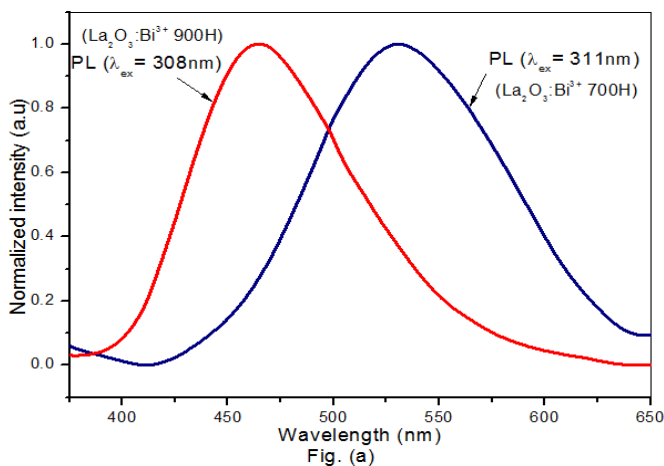


Fig. 6 (a)TEM image (b) HRTEM of 900 °C $\text{La}_2\text{O}_3:\text{Bi}^{3+}, \text{Tb}^{3+}$ phosphors material

Fig.5 (a) and (b) represents TEM, HRTEM image of $\text{La}_2\text{O}_3:\text{Bi}^{3+}, \text{Tb}^{3+}$ sample after heating at 700 °C were obtained which indicates the created oxides are nanocrystalline materials with the average crystalline grain size of about 40-50nm which slightly more when compared with size calculated from Scherrer's relation in XRD. When the temperature was further increased to 900 °C, the nanoparticles became bigger and merged with each other, and the sharpness of the particles completely vanished. The merging is related to the melting process because the surface-to-volume ratio of the nanoparticles is relatively high, and at high temperatures, the surface energy substantially affects the interior bulk properties of the materials. Fig. 6 (a & b) shows TEM, HRTEM image of 900 °C.

3.3 PL studies from 1 at% Bi doped La_2O_3 powder phosphors



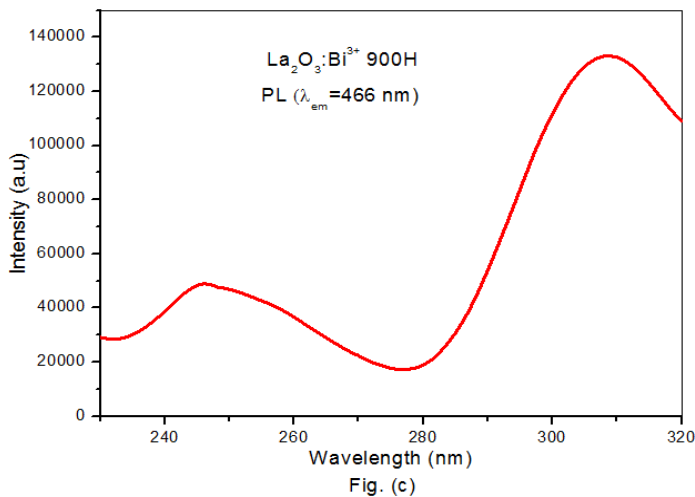


Fig.6 PL emission spectra (a) $\text{La}_2\text{O}_3:\text{Bi}^{3+}$ 700 and 900 °C heated samples (b) PL excitation spectra $\text{La}_2\text{O}_3:\text{Bi}^{3+}$ 700 °C heated and (c) PL excitation spectra $\text{La}_2\text{O}_3:\text{Bi}^{3+}$ 900 °C heated samples.

Blue emission from $\text{La}_2\text{O}_3:\text{Bi}^{3+}$ phosphor thin film has been previously reported[27–29]. The emission spectra of 700 and 900 °C heated $\text{La}_2\text{O}_3:\text{Bi}^{3+}$ powder samples are shown Fig.6(a).The emission peak maximum at 528nm of 700 °C heated sample under excitation of 311nm is observed and corresponding excitation spectra is shown in Fig.6 (b). As for the 900°C sample it is observed a blue shift in emission peak at 466nm and increase in emission intensity when excited at 308nm. During sintering, excited luminescent centers are thermally activated through phonon interactions, which cause thermal release through the crossing point between the excited and ground states according to a configuration coordinate diagram [30]. At higher temperature, the density of phonons increases, and electron-phonon interactions dominate, so a blue shift of the emission band is observed for the phosphors as the temperature increases which is in accord with the reported thin film $\text{La}_2\text{O}_3:\text{Bi}^{3+}$ phosphor[31].In general, the temperature dependence of phosphors used in phosphor-conversion white LEDs is important because it has a considerable influence on the light output and color rendering index. From Fig.6 (c) the excitation spectra of 900 °C consists of two bands, the main excitation band peaks around 308 nm and the weak band peaks around 250 nm, originating from the $6s^2-6s6p$ transition in Bi^{3+} .

The lifetime value is found to be significantly lower (0.9 μs) for 700 °C heated sample when compared to the 900 °C sample (8.2 μs) which can be seen from the decay curve shown in Fig. 7 (a,b) This is explained based on the general expression for the oscillator strength of an electronic transition (f_{ex}), as given by equation 1, [32]

$$f_{ex} = \frac{2m}{\hbar} \Delta E |\mu|^2 |U(0)|^2 \dots\dots\dots (1)$$

Where ΔE is the transition energy, μ is the transition dipole moment and $|U(0)|^2$ is the probability of finding an electron and hole at the same place, m is the effective mass of electron, and \hbar is Planks constant. For nanoparticles, due to their small size, the term, $|U(0)|^2$ is much higher compared to corresponding bulk and hence will have higher transition probability with respect to bulk. Higher oscillator strength (f_{ex}) values suggest shorter excited state lifetime, as both are inversely related. This accounts for the observed decrease in the lifetime values for the 700 °C samples compared to corresponding 900 °C samples. Since the decays are multi exponential average lifetime values are calculated and used for comparison.

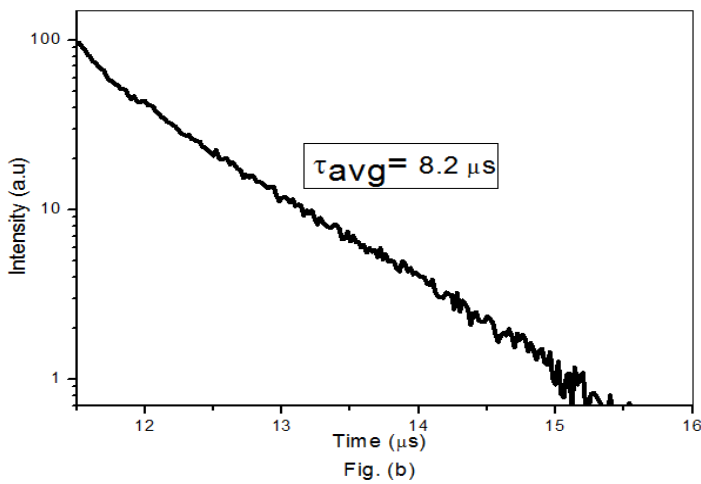
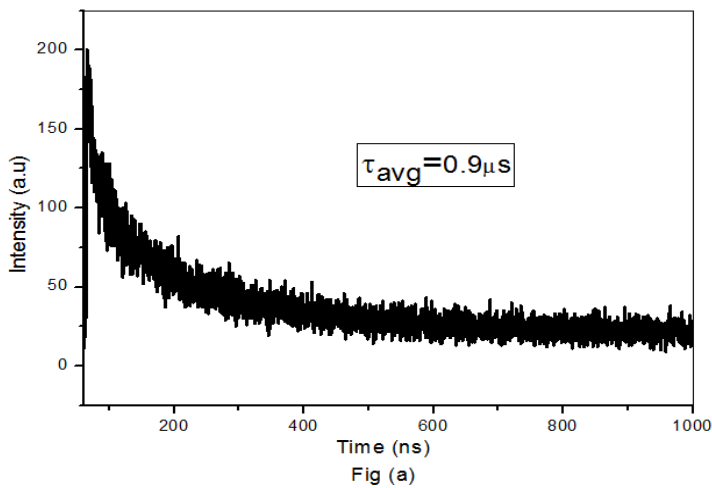


Fig.7 Decay curves corresponding to (a) $\text{La}_2\text{O}_3:\text{Bi}^{3+}$ (700 °C) heated and (b) $\text{La}_2\text{O}_3:\text{Bi}^{3+}$ (900 °C) heated samples.

3.5 PL studies from $\text{La}_2\text{O}_3:1 \text{ at}\% \text{ Bi}, 1 \text{ at}\% \text{ Tb}$ powder phosphor

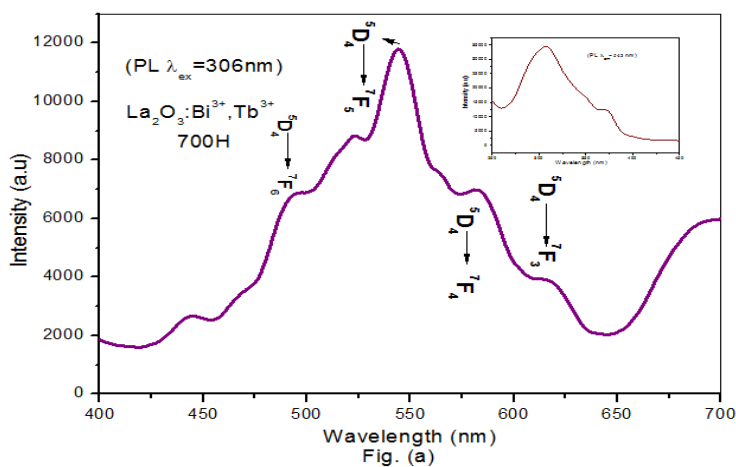


Fig.8(a,b) shows the excitation and emission spectra of the 700 °C and 900 °C heated Tb^{3+} co-doped (1 at %) samples. The excitation spectra (Fig. 9(a)) for 700 °C heated was obtained at an emission wavelength of 543

nm, which corresponds to the direct $^5D_4 \rightarrow ^7F_5$ transition of Tb^{3+} . A weak excitation peak was observed at 370 nm, which were assigned to the $^5D_3 \leftarrow ^7F_6$ transitions of Tb^{3+} . Broad excitation peak at 306 nm, which is assigned to the $^4f_8 \leftarrow 4f_7, 5f_1$ transitions [33]. For the emission spectrum at an excitation wavelength of 306 nm, corresponding to the direct $^5L_{10} \leftarrow ^7F_6$ transitions of Tb^{3+} , the emission peaks were observed at 491, 546, 586, and 621 nm, which were assigned to the $^5D_4 \rightarrow ^7F_J (J = 6, 5, 4, \text{ and } 3)$ transitions, respectively [34–40]. Upon heating to 900 °C, the emission (Fig. 8 (b)) intensity increased dramatically due to the removal of quenching sites and an increase in crystallinity, as discussed above.

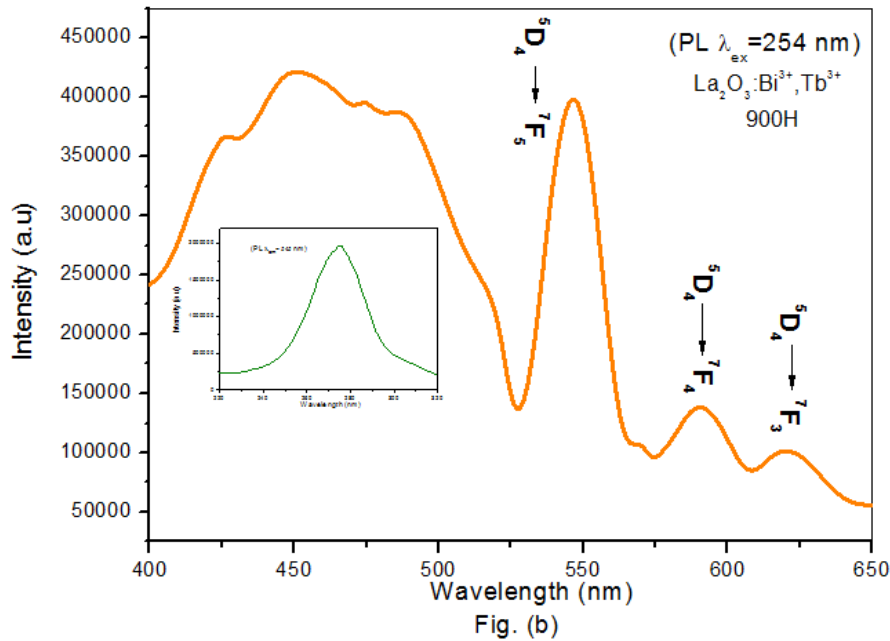


Fig.8 Emission and Excitation (inset) (a) $La_2O_3:Bi^{3+}, Tb^{3+}$ (700 °C) heated and (b) $La_2O_3:Bi^{3+}, Tb^{3+}$ (900 °C) heated samples

Although the emission profile was similar to that of the 700 °C sample, the excitation profile was changed more critically, where Tb–O charge transfer band peak at 275 nm is observed. Here it is observed that at 700 °C heated sample the $La_2O_3:Bi^{3+}$ host emission is very weak as compared to the 900 °C and as a result it is understood that efficient energy transfer from Bi^{3+} to Tb^{3+} is more in 900 °C sample which also supported by the life time decay curve values as shown in Fig.9 (a,b)

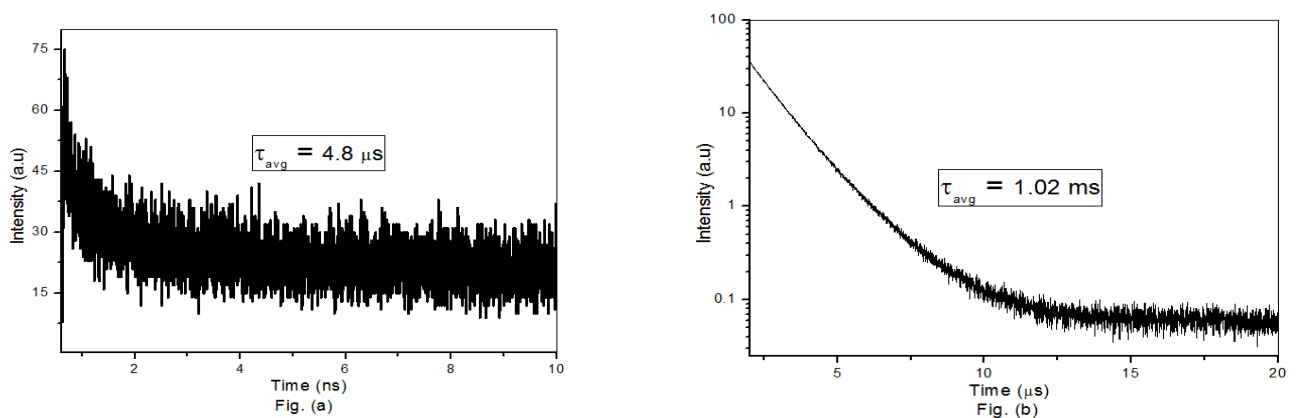


Fig.9 Decay curves corresponding to (a) $La_2O_3:Bi^{3+}, Tb^{3+}$ (700 °C) heated and (b) $La_2O_3:Bi^{3+}, Tb^{3+}$ (900 °C) heated samples.

3.7 FTIR Spectra

FT-IR spectrum of as-prepared dried samples recorded from 400 to 4000 cm^{-1} shown in Fig.10. The as prepared (undoped) La_2O_3 spectrum Fig.(a) shows an sharp band at 3614 cm^{-1} , corresponding to the stretching and bending O–H vibrations [41] and absorption band at 3481 cm^{-1} results from the O–H vibration of H_2O absorbed by the nanoparticles. The strong broad band at 1450 cm^{-1} is attributed to C-H bending. The FT-IR spectrum is in good agreement with the XRD pattern of as prepared La_2O_3 . Whereas from the spectra Fig.(b and c) of $\text{La}_2\text{O}_3:\text{Bi}^{3+}$ doped and Tb^{3+} co-doped samples it is clearly shows the absence of sharp peak at 3614 cm^{-1} [42,43]. The weak absorption band peak observed at O-H vibration of water molecules that are absorbed by bismuth doped nanoparticles at 3471 cm^{-1} and weak broad band assigned at 3462 cm^{-1} for co-doped samples. A medium C-H bond stretching is observed at 2892 cm^{-1} and two peaks were commonly observed at 1384 and 1464 cm^{-1} , which were assigned C-H bending, respectively in all doped La_2O_3 nanoparticles. Hence, the doped Bi^{3+} and rare earth ions are soluble in ethylene glycol (EG) homogenously by forming steady metal complexes due chelation between metal ions and EG which is verified from IR spectra.

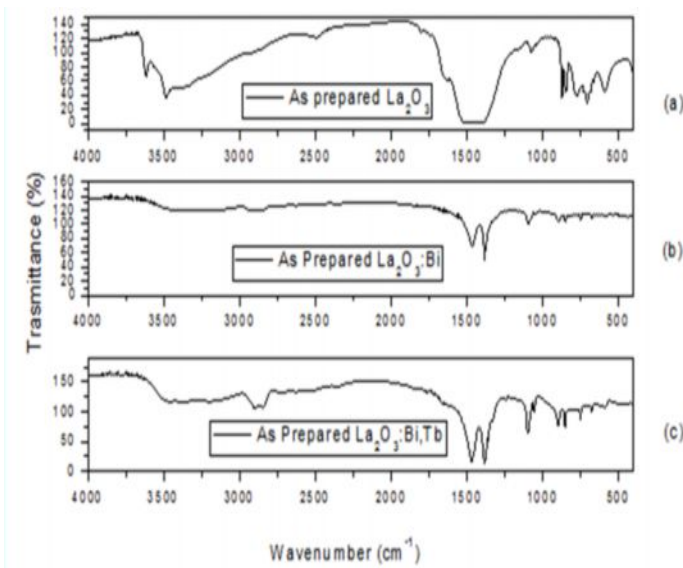


Fig. 10 FTIR spectra of As Prepared $\text{La}_2\text{O}_3:\text{Bi}^{3+}, \text{Tb}^{3+}$

3.8 CIE Coordinates

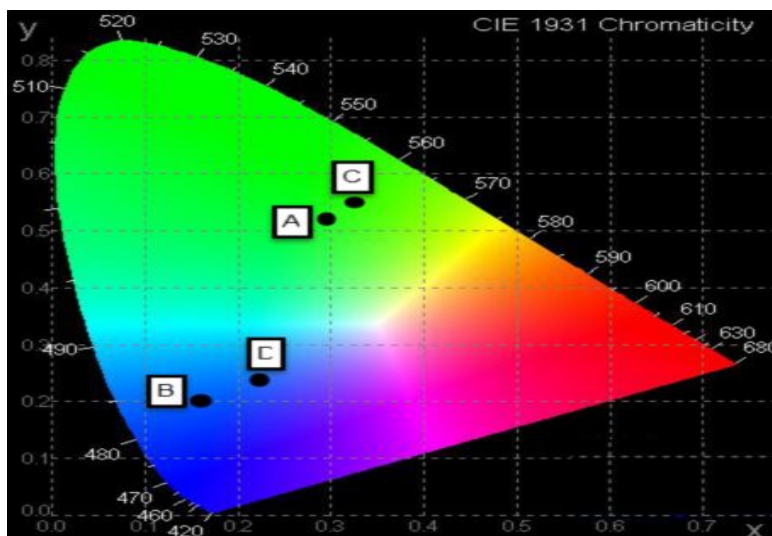


Fig. 11 CIE chromaticity color coordinates in PL emissions from 700 °C and 900 °C heated $\text{La}_2\text{O}_3:\text{Bi}^{3+}$ and Tb^{3+} co-doped samples.

The color of PL emissions observed from $\text{La}_2\text{O}_3:\text{Bi}^{3+}$, Tb^{3+} powder samples changed to blue from green as the temperature of the powder increased. Fig.11 shows the CIE chromaticity color coordinates of PL emissions from $\text{La}_2\text{O}_3:\text{Bi}^{3+}$, Tb^{3+} phosphor. The color change in PL emission observed from $\text{La}_2\text{O}_3:\text{Bi}^{3+}$, Tb^{3+} phosphor material is explained as the result that the energy of excited electrons has efficiently transferred from the excited state of Bi^{3+} to that of Tb^{3+} ion. CIE colour coordinates have been calculated and found to be (0.30, 0.51), (0.16, 0.20), (0.32, 0.52), (0.22, 0.26), respectively for $\text{La}_2\text{O}_3:\text{Bi}^{3+}$ (700 °C), $\text{La}_2\text{O}_3:\text{Bi}^{3+}$ (900 °C), $\text{La}_2\text{O}_3:\text{Bi}^{3+}$, Tb^{3+} (700 °C), $\text{La}_2\text{O}_3:\text{Bi}^{3+}$, Tb^{3+} (900 °C) respectively.

4.0 Conclusion

In this paper we have successfully synthesized Bi^{3+} doped and Tb^{3+} co-doped La_2O_3 nanophosphors material by polyol method. The XRD patterns exhibited a hexagonal structure, and the FTIR spectra confirmed the presence of OH^- group in all as prepared La_2O_3 undoped and doped samples. After heating, the as prepared La_2O_3 and $\text{La}_2\text{O}_3:\text{Bi}^{3+}$ and Tb^{3+} co-doped samples, the XRD pattern confirmed the formation of the pure La_2O_3 hexagonal phase. The effect of heating and doping on the morphology of $\text{La}_2\text{O}_3:\text{Bi}^{3+}$ doped and Tb^{3+} co-doped were also examined by SEM and TEM images. All the observed emission peaks in PL from $\text{La}_2\text{O}_3:\text{Bi}$, Tb^{3+} phosphor powder were assigned to either the broad emission originating from the transition in Bi^{3+} or the visible emission peaks originating transition from the Tb^{3+} ions. The shifting of emission from the samples on heating is clearly observed from the CIE color coordinates plot. Finally, from the above studies, we are able to suggest that the $\text{La}_2\text{O}_3:\text{Bi}^{3+}$, Tb^{3+} nanophosphors powders are promising materials for application in the development of novel optical systems such as FEDs, plasma display panels.

Acknowledgements

One of the authors (K.Ramachandra Rao) is grateful to the UGC-SERO, Government of India for sanctioning the minor research project (No.F MRP-4500/14). The authors express their gratitude towards Dr.V.Sudarsan, BARC, Mumbai for providing Photoluminescence studies. Our sincere thanks to Dr.Ch.Masthanaiah, Principal, Government College (A), Rajahmundry for providing necessary research lab facilities.

References

1. Van Steensel.L.I, Bokhove S.G., van de Craats A.M., de Blank J., Blasse G., Mater. Res.Bull, 1995,30,1359.
2. Shin S.H., Jeon D.Y., Suh K.S., J. Appl. Phys, 2001, 90, 5986.
3. Liu,X.M. Lin.J, J. Lumin, 2007,700,122–123.
4. Fukada.H, Sahara.K, Ishino.J, T. Miyata, T. Minami, Proc. of the 16th Int. DisplayWorkshops, 2009,371.
5. Fukada.H,Konagai.M,Ueda.K, Miyata.T, Minami.T, Thin Solid Films,2009,517 ,6054.
6. W.M. Yen, M.J. Weber, Inorganic Phosphors, CRC Press, New York, 2004.
7. Datta.R.K, J. Electrochem. Soc., 1967, 114,1137.
8. Blasse.G,Bril.A, J. Chem. Phys.,1968,48 217.
9. Kale.S.S, Jadhav.K.R, Patil.P.S, Gujar.T.P,Lokhande.C.D, Mater. Lett, 2005, 59, 3007.
10. Wu.Y.H, Yang.M.Y,Chin.A, Chen.W.J,Kwei.C.M, IEEE Electron Dev. Lett. 2000,21, 341.
11. Koehler.W.C, Wollan.E.O, ActaCryst, 1953,6, 741.
12. Valange.S,Beauchaud.A,Barrault.J, Gabelica.Z, Daturi.M, Can.F, J. Catal.2007, 251, 113.
13. Bluthardt.C, Fink.C, Flick.K,Hagemeyer.A, Schlichter.M, Volpe Jr..A, Catal.Today ,2008, 137, 132.
14. Neumann.A,Walter.D, Thermochim. Acta,2006, 445, 200.
15. Deng.J, Zhang.L, Au.C.T, Dai.H, Mater. Lett. 2009, 63, 632.
16. Ma.X, Zhang.H, Ji.Y, Xu.J,Yang.D, Mater. Lett.,2004,58, 1180.
17. Liu.J,Fei.X.Y, Yu.X.B, Tao.Z.W, YangL.Z, Yang.S.P, J.Non-Cryst.Solids, 2007,353,4697.
18. Mendez.M, Carvajal.J.J,Cesteros.Y,Aguilo.M, Diaz.F, Giguere.A, Drouin.D, Ferrero.E.M,Salagre. P,Formentin.P, Pallares.J, Marsal.L.F, Opt.Mater,2010,32, 1686.
19. .Liu.X.M,Yan.L.S,Zou.J.P,J.Electrochem.Soc.2010, 157, P1.
20. Ying Zhang, Muying Wu, Zhang.W.F,Modern Physics Letters B, 2010, Vol. 24, Nos. 4 & 5, 475–485.

21. Toshihiro Miyata, Jun-ichi Ishino, Keiichi Sahara, Tadatsugu Minami, Thin Solid Films, 2011, 519, 8095–8099
22. Lui. H, Wang.L, Chen.S, Zuo.B, J. Lumin, 2007, 126, 459.
23. Liu.H.Q, Wang.L.L, Huang.W, Peng.Z.W, Mater. Lett, 61 (2007) 1968.
24. Liu.X.M, Yan.L.S, Zou.J.P, J. Electrochem. Soc., 2010, 157, P1.
25. Li.G.G, Peng.C, Zhang.C.M, Xu.Z.H, Shang.M.M, Yang.D.M, . Kang.X.J, Wang.W.X, Li.C.X, Cheng.Z.Y, J. Lin, Inorg. Chem. 2010, 49, 10522.
26. Koehler.W.C, Wollan.E.O, Acta Cryst. 1953, 6, 741.
27. Yen.W.M, Weber.M.J, Inorganic Phosphors, CRC Press, New York, 2004.
28. Datta.R.K, J. Electrochem. Soc, 1967, 114, 1137.
29. Blasse.G, Brill.A J. Chem. Phys, 1968, 48, 217.
30. Kim J S, Park Y H, Kim S M, et al. Solid State Commun, 2005, 133: 445–448.
31. Knox.R.S, Theory of Excitons, Solid State Physics Supplements, Academic Press, New York, 1963
32. Jia.G, Huang.Y, Song.Y, Yang.M, Zhang.L, You.H, Eur. J. Inorg. Chem. 2009, 25, 3721–3726.
33. Cho.I, Kang.J.G, Sohn.Y.G, J. Lumin, 2015, 157, 264–274.
34. Sohn.Y, Ceram. Int, 2014, 40, 13803–13811.
35. Kim.W.J, Gwag.J.S, Kang.J.G, Sohn.Y, Ceram. Int, 2014, 40, 12035–12044.
36. Cho.I, Kang.J.G, Sohn.Y, Bull. Korean Chem. Soc, 2014, 35, 575–580.
37. Sohn.Y, Ceram. Int, 2014, 40, 2467–2475.
38. Choi.Y.I, Sohn.Y, RSC Adv. 4, 2014, 31155–31161.
39. Sohn.Y, Ceram. Int, 2013, 39, 9157–9161.
40. Shionoya.S, Yen.W.N, Phosphor Handbook, CRC Press, New York, 1999.
41. Khaja Hussain.Sk, Nagaraju.Goli, Pavitra.E, Seeta Rama Raju. Gand Jae Su Yu Cryst Eng Comm, 2015, 17, 9431.
42. Jie Liu, Xiaoyan Fei, Xibin Yu, Zhenwei Tao, Liangzhun Yang, Shiping Yang Journal of Non-Crystalline Solids, 2007, 353, 4697–4701
43. Lixin Song, Pingfan Du, Jie Xiong, Xiaona Fan, Yuxue Jiao. J. Lumin, 2012, 132, 171–174.
